International Journal of Greenhouse Gas Control 156 (2026) 104796

Contents lists available at ScienceDirect

International Journal of Greenhouse Gas Control

journal homepage: www.elsevier.com/locate/ijggc

Induced seismicity at the Quest Carbon Capture and Storage project, Alberta

James P. Verdon *, Cindy S.Y. Lim, Germán Rodríguez-Pradilla

School of Earth Sciences, University of Bristol, Bristol, United Kingdom

ARTICLE INFO

Keywords:
Induced seismicity
Carbon capture and storage

ABSTRACT

The 1st April and 9th May 2026 $M_L \geq 4.0$ earthquakes in central Alberta were felt across the city of Edmonton. The events were located near to Carbon Capture and Storage (CCS) operations at the Quest site. In this study we use an established induced seismicity assessment framework, applied with respect to the Quest CCS site as well as other oilfield activities in the area, to assess whether the events were induced. We found that these earthquakes were likely caused by CO_2 injection at Quest, making this the first known example of felt induced seismicity caused by CCS operations. We have inverted regional seismic monitoring data to compute event depths and source mechanisms, finding that the events were located in the upper portion of crystalline basement, with oblique strike-slip/reverse focal mechanisms. We apply several induced seismicity magnitude forecasting schemes to the earthquake sequence in order to evaluate whether the seismic hazard posed by these events could have been identified. We found that two models – the seismogenic index model and a model based on extreme value theory – would both have forecasted the M_L 4.0 events prior to their occurrence. These results demonstrate that induced event forecasting methods can be used to support operational decision-making. We conclude by considering options for ongoing induced seismicity hazard mitigation, both at the Quest CCS site, and more generally at any future CCS operations.

1. Introduction

Induced seismicity is created when subsurface industrial operations perturb the stress state on tectonic faults, generating earthquakes. Induced seismicity has been associated with many different types of subsurface industry, including hydraulic fracturing for shale gas, stimulation of geothermal reservoirs, depletion and compaction of mature hydrocarbon reservoirs, injection of methane for natural gas storage, and subsurface wastewater disposal (WWD). The occurrence of induced seismicity can pose a nuisance for the public who experience shaking caused by induced earthquakes (e.g., Cremen and Werner, 2020), and in extreme cases induced seismic events have reached sufficient magnitude to cause damage to nearby buildings and infrastructure (e.g., Lee et al., 2019; Campbell et al., 2020).

Regulators have typically responded to cases of induced seismicity by imposing requirements for operators to manage induced seismicity hazard by, for example, reducing wellhead pressures and injection volumes (e.g., OCC, 2016), or halting operations altogether (e.g., van de Graaff et al., 2018; BEIS, 2019). Operators may be expected to conduct induced seismicity risk assessments before commencing subsurface activities that are known to be prone to induced seismicity (e.g., AER, 2026), and to follow Traffic Light Scheme (TLS) protocols to respond to ongoing induced seismicity (Verdon and Bommer, 2021).

1.1. Induced seismicity, microseismicity, and CCS

The potential for Carbon Capture and Storage (CCS) projects to generate induced seismicity has long been recognised (e.g., Zoback and Gorelick, 2012; Verdon, 2014; Zoback and Hennings, 2025). High resolution "microseismic" monitoring arrays at CCS sites have previously identified small-magnitude events that have generally not been of sufficient magnitude to be felt (e.g., Verdon et al., 2011; 2013; Stork et al., 2015; Dando et al., 2021; Goertz-Allmann et al., 2024). However, numbers and magnitudes of induced seismic events are widely recognised to scale with the volumes of fluid injected into the subsurface (Shapiro et al., 2010; Hallo et al., 2014; van der Elst et al., 2016; Verdon et al., 2024). As such, as the numbers of operational CCS projects, and the scale of individual projects, have grown, effective management of

* Corresponding author.
E-mail address: James.Verdon@bristol.ac.uk (J.P. Verdon).

https://doi.org/10.1016/j.ijggc.2026.104796
Received 1 July 2026; Received in revised form 14 September 2026; Accepted 14 September 2026
Available online 22 September 2026

induced seismicity is increasingly becoming an important issue for the nascent CCS industry.

Note that in this study, we use the term "induced" to refer to any earthquakes caused by industrial activities in the subsurface, and do not seek to differentiate between "triggered" earthquakes – where the bulk of seismic energy released is stored tectonic energy, with the industrial operation serving to nucleate the events – and "driven" earthquakes – where the bulk of seismic energy released was imparted directly by the industrial operations (Bommer and Verdon, 2024).

Several commercial-scale CO_2 injection projects (either for CCS or Enhanced Oil Recovery, EOR, or a combination of both) have recorded induced seismicity and microseismicity (Hosseini et al., 2022), though to date the events been of very small magnitude in the majority of cases. At the Weyburn CCS-EOR project in Saskatchewan, the microseismic response to injection was very low, with approximately 200 events detected over eight years of monitoring, the magnitudes of which did not exceed M_W -0.5 (Verdon, 2016). At the Ketzin CCS pilot site in near to Potsdam, Germany, a small number of microseismic events were recorded, with the largest reaching M_L 0.5 (Paap et al., 2014). Several phases of injection and microseismic monitoring have been conducted at the Otway CCS test site in Victoria, southern Australia, and the largest events have been below M_W 0 (Glubokovskikh et al., 2022).

Over 6,000 microseismic events were recorded during injection of CO_2 at the Lacq-Rousse field in southern France, with the largest magnitudes reaching M_W -0.5 (Payre et al., 2014). Significantly larger earthquakes, up to M_L 4, have been linked to previous gas production and WWD activities in the Lacq field (Grasso et al., 2021; Jacquemond et al., 2024). At the Aneth CCS project in Utah, over 1,000 microseismic events were detected, with the largest having a magnitude of M_W 0.8: these events were, however, associated with a deeper WWD well at the site, rather than the CO_2 injection itself (Rutledge and Soma, 2010). At the Decatur CCS project in Illinois, over 5,000 microseismic events have been detected, with the largest reaching M_W 1.2 (Dando et al., 2021). At In Salah, over 9,000 microseismic events have been detected, with the largest events reaching M_W 1.7 (Stork et al., 2015). These events were associated with significant surface uplift and opening of fracture networks within the reservoir (Verdon et al., 2015). At the Gorgon CCS Project offshore NW Australia, the largest reported event has reached M_W 2.3 (Langenbruch and Shapiro, 2025), though little public information is available regarding this case.

The Cogdell oilfield in northwest Texas is often cited as the most significant case of seismicity caused by CO_2 injection to date. The Cogdell field first experienced induced seismicity in the 1970s with magnitudes exceeding M_L 4 associated with water injection for EOR (Davis and Pennington, 1989). Seismicity then subsided through the 1980s and 1990s, but saw a resurgence in the 2000s, with the largest event reaching M_W 4.4 in 2011. Gan and Frohlich (2013) concluded that the resurgence in seismicity was caused by the combined influence of water, methane and CO_2 injection in the field for tertiary oil recovery.

1.2. Felt Seismicity in the NE edmonton area

The 1^{st} April 2026 M_L 4.0 and 9^{th} May 2026 M_L 4.2 earthquakes, with epicentres to the NE of Edmonton, Alberta, are located within 10s of km of the Quest CCS project, where CO_2 captured at a nearby heavy oil processing facility is injected into a deep aquifer for disposal. These events were widely felt by the public across the city of Edmonton (CTV, 2026). If induced by operations at Quest, this seismicity would represent the first reported case of felt induced events caused by CCS. They are therefore of great significance, posing a challenge to our ability to manage induced seismicity risks during CCS operations.

In this paper we examine the seismicity in the vicinity of the Quest site and its relationship with subsurface industrial operations in the area (including the Quest CCS project and other oilfield activities). We use an established induced seismicity attribution scheme to ascertain whether the events are natural or induced, finding that the most likely conclusion is that the events have been induced by CCS operations at Quest.

Having established that the seismicity is likely induced by CCS operations, we apply various models that have been developed to forecast the magnitudes of induced seismicity sequences and evaluate their ability to forecast the increase in seismic magnitudes observed in 2026 at the Quest site. We conclude by making recommendations with regards to the management of induced seismicity risks at future CCS sites.

2. Subsurface industrial operations

Fig. 1a shows a map of the major subsurface industrial activities taking place in the region of interest, along with earthquakes reported by the Alberta Geological Survey (AGS, 2020). The two principle subsurface activities taking place in the area include CO_2 injection at the Quest site, and conventional oil production under waterflooding at the Redwater oilfield. Fig. 1b shows a timeline of CO_2 injection at Quest and water reinjection for secondary oil recovery at Redwater with respect to the reported seismicity. Given the co-location of CCS and oilfield operations, it is necessary to perform a detailed assessment in order to determine whether the observed seismicity is induced, and if so, which industrial activities may have contributed to the seismicity.

2.1. CCS at Quest

At the Quest site, CO_2 is captured at the Scotford Upgrader plant, to the north of Edmonton, and injected via deep wells into the subsurface. Injection began in 2015, and over 10 million tonnes of CO_2 have been stored, at an average rate of approximately 1 million tonnes per year. Injection is into the Basal Cambrian Sandstone (BCS) aquifer at a depth of around 2 km below surface, via three injection wells spaced approximately 6 km from each other. Fig. 1a shows the position of the Quest Sequestration License Area (QSLA) and the CO_2 injection wells.

The BCS in this region has a thickness of 40 – 50 m, a porosity of 16 %, and the permeability ranges between 20 – 500 mD (Shell Canada, 2015). The BCS sits directly on top of the underlying Precambrian crystalline basement. The primary caprock seal for CO_2 containment includes shales within the overlying Deadwood Formation, which in turn are overlain by the Lower and Upper Lotsberg salt formations, and the Prairie Evaporite (see Fig. 2). Further barriers to upward CO_2 migration are provided by additional aquitards in the overburden. No faults penetrating the caprock complex were observed in 2D or 3D seismic surveys at the Quest site (Shell Canada, 2015). However, structural lineaments at the top of the underlying basement have been identified in geophysical surveys (Shell Canada, 2025a). We are not aware of any evidence to indicate that the injected CO_2 has migrated beyond the target storage complex.

2.2. Oil production under waterflooding at Redwater

The Redwater oilfield is a mature, conventional oilfield. The field was discovered in 1948, and production began in 1953. In total, the field has produced approximately 1 billion barrels of oil. The Redwater oilfield is found in the Devonian-age Leduc reef complex at a depth of approximately 1 km below surface (Fig. 2). Co-produced water is reinjected into the reservoir unit in order to maintain pressures and support hydrocarbon recovery. The Leduc Formation is separated from the underlying BCS (the target for CCS at Quest) by the hydrogeological barriers described in Section 2.1 (the Lotsberg salts and the Prairie Evaporite). The net volume change at Redwater is negative (i.e., more fluid has been extracted than injected, since oil and water are produced, with the produced water being re-injected).

3. Seismicity

A dedicated microseismic monitoring array has been installed at the Quest site (Goertz-Allmann et al., 2024), however data from this array is

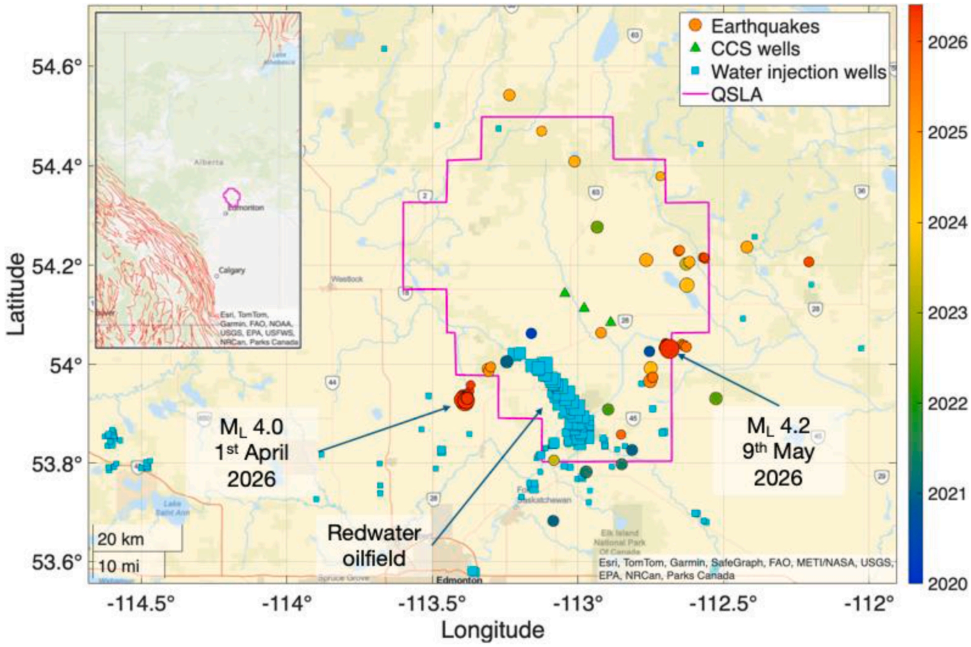

(a)

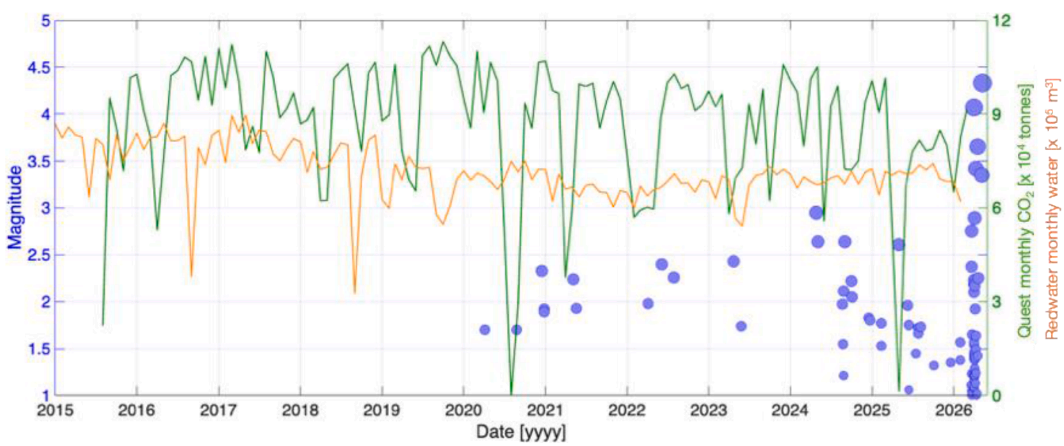

(b)

Fig. 1. Map (a) and timeline (b) of subsurface industrial activities in the region surrounding the Quest CCS project. In (a), the earthquakes are coloured by occurrence date and sized by magnitude. Water injection wells are sized by cumulative injected volume. The $M_L \geq 4.0$ earthquakes are marked. The inset map shows the position of the QSLA within Alberta, along with the positions of mapped faults (red lines).

proprietary and does not form part of this study. We nonetheless note that the first reported microseismic events at Quest occurred in 2016, and the first $M_W \geq 0.0$ events were reported in 2017 (Shell Canada, 2025b). Regional seismic monitoring is provided by the Alberta Geological Survey (AGS, 2020), primarily using data from the RAVEN and SCISMN arrays (Schultz and Stern, 2015; Schultz et al., 2020). The first events in the AGS catalogue were observed in 2020, with magnitudes less than M_L 2.0. Both the rate and magnitudes of the observed earthquakes have increased since then, culminating in the $M_L \geq 4.0$ events in April and May 2026. In the following section, we use the seismic data recorded by regional monitoring stations (Fig. 3) to further constrain the hypocentres and source mechanisms for the largest events. These observations provide important information with respect to assessing induced seismicity causation in Section 4. For the seismic hazard assessments presented in Section 5, we use the regional earthquake catalog as reported by the AGS. Fig. 3 shows the seismic stations from which we sourced waveform data in the following analyses.

3.1. Mainshock depths and source mechanisms

Event focal depths and source mechanisms are important factors in determining whether earthquakes are induced or natural (Verdon et al., 2019). For induced events, event depths and focal mechanisms can provide important information in order to understand the geomechanical processes that may be at play in triggering the seismicity (e.g., Igonin et al., 2021; 2022; Verdon et al., 2026).

We use Grond (Heimann et al., 2018) to determine focal depths and deviatoric moment tensor solutions for the 1st April 2026 M_L 4.0 and 9th May 2026 M_L 4.2 earthquakes. Grond is an open-source Python package that performs Bayesian bootstrap-based probabilistic joint inversion of regional waveform data to estimate earthquake source parameters. The inversion minimises the misfit between the modelled and observed

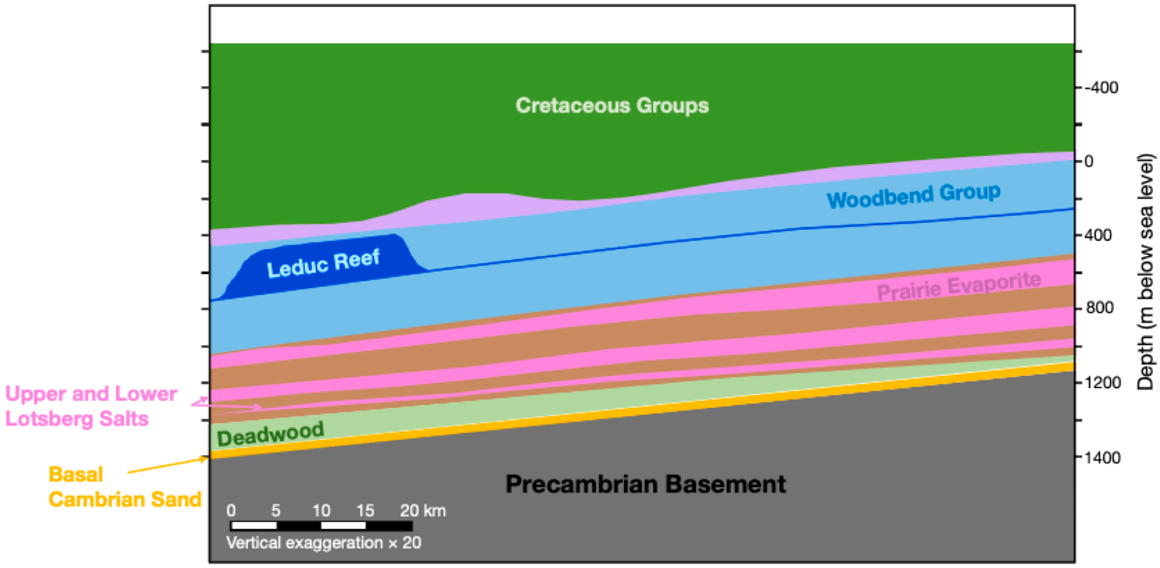

Fig. 2. Schematic cross-section representing the key geological features at the Quest CCS site. Adapted from (Shell Canada, 2013).

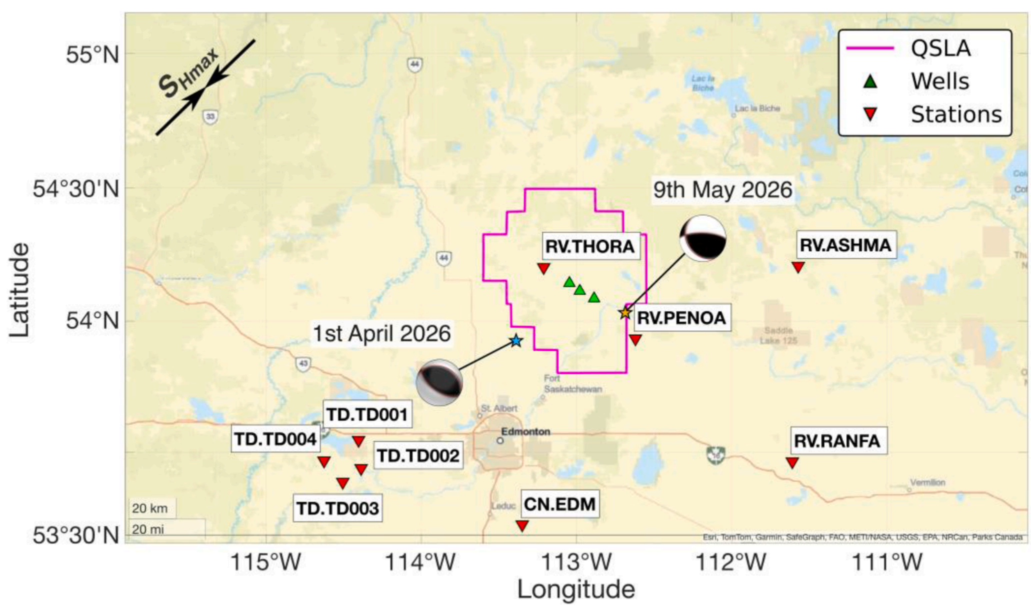

Fig. 3. Map showing the regional seismic monitoring stations used for our event re-location and focal mechanism analysis. The fuzzy double-couple (DC) moment tensor solutions for the 1st April and 9th May $M_L \geq 4.0$ events are shown as beachball diagrams, plotted at their epicentral locations. The S_{Hmax} orientation is indicated.

waveforms recorded on the regional monitoring stations (Fig. 3). Following Yu et al. (2022), we accept the final moment tensor solution when: (i) the modelled waveforms are well fitted at a sufficient number of stations (we use ≥ 50%); (ii) the nodal plane parameter solutions fall within the 90% confidence intervals of the probability distribution functions (PDFs); and (iii) the double-couple solutions are consistent and show a clustered spatial distribution. Further details of the Grond setup, waveform processing and full moment tensor solutions for both events are provided in the Supplementary Materials (Section S1 and Figures S1-S3).

The best-fitting double-couple (DC) solutions indicate reverse faulting for the 1st April event and oblique reverse faulting for the 9th May event (Table 1), at focal depths (below surface) of 3.6 km and 4.6 km, respectively, with the 5 % to 95 % confidence intervals for each event ranging from 2.8 – 4.5 km and 4.3 – 5.6 km, respectively. These locations (and the associated uncertainties) place both events within the upper part of the Precambrian basement. Table 1 lists the orientations of the nodal planes for both events. These focal mechanisms are consistent

Table 1
Focal mechanism solutions from the moment tensor inversions for the 1st April 2026 M_L 4.0 and 9th May 2026 M_L 4.2 earthquakes. This table also shows the moment magnitude and depths derived for each earthquake. Strike, dip and rake are given for both nodal planes (NP1/NP2).

Date & Time (UTC)	Strike (°)	Dip (°)	Rake (°)	Moment magnitude, M_w	Depth (km)
1st April 2026, 23:27:29	291/ 127	30/ 61	76/98	3.98	3.6
9th May 2026, 15:05:05	273/ 148	72/ 30	66/ 141	4.01	4.6

with the N46°E (NE-SW) maximum horizontal stress orientation, S_{Hmax} in the Alberta basin (Reiter et al., 2014) and broadly align with the NW-SE trending regional thrust faults from the Rocky Mountains (McCafferty et al., 2025) (see Fig. 1a inset).

4. Induced seismicity attribution

We use the induced seismicity attribution framework developed by Verdon et al. (2019) to assess whether the earthquakes are natural or induced, and if induced, what subsurface activities are causing them. We apply the attribution framework to the two subsurface industrial operations taking place in the area, as described in Section 2.

The Verdon et al. (2019) framework poses a series of questions with weighted scores that are summed to produce the Induced Assessment Ratio (IAR): a positive IAR implies that the event is induced, a negative IAR implies that the event is natural, and an IAR close to zero implies that the evidence is ambiguous. Crucially, the Verdon et al. (2019) framework also allows the user to consider the quality of the available evidence via the Evidence Strength Ratio (ESR): a low ESR implies that the quality of evidence used in the assessment is weak, while a high ESR implies that the evidence used in the assessment is strong. Table 2 shows our responses to the assessment questions, and Table 3 lists the resulting ESR and IAR scores. Further notes for each question are provided in the Supplementary Materials (Section S2).

We find that the ESR for both potential causes is high, indicating that most of the evidence needed to perform an induced seismicity attribution assessment is available. Potential improvements to the available data could include: history-matched full-field reservoir simulations in order to better constrain the pressure changes caused by the different activities; improved reflection seismic coverage to image faults near to the large earthquakes (3D seismic coverage is only available around the CCS injection wells); and an improved microseismic catalog to assess in more detail the temporal and spatial evolution of seismicity relative to subsurface operations.

The IAR for CCS operations at Quest is clearly positive, and we conclude that this activity is likely to be the cause of the events in question. The swarm-like nature of the seismicity, and the ongoing elevated rates over a period of more than six years has only been observed for other sequences of induced seismicity in the West Canadian Sedimentary Basin (WCSB), but not for natural earthquakes. The seismicity commences shortly after the onset of CO_2 injection and has grown in magnitude as CO_2 injection has continued. The event locations are within the expected footprint pressure plume caused by CO_2 injection (Shell Canada, 2015), and there is a plausible hydrological or geomechanical connection from the BCS into the underlying basement where the events occurred, with structural lineaments observed at the basement horizon near to the CCS injection wells (Shell Canada, 2025a).

However, while there is a qualitative link between the CO_2 injection and the growing levels of seismicity, we did not observe a strong statistical correlation between injection rates and the seismicity (in contrast to, for example, Oprsal and Eisner, 2014; Schultz and Telesca, 2018; Verdon et al., 2026). Likewise, the locations of the seismicity have not shown a progressive outward growth from the CO_2 injection wells, as might be expected if the induced seismicity were being triggered by an expanding pressure pulse that is progressively intersecting critically stressed faults. This implies a more complex geomechanical mechanism for triggering the seismicity such that simple temporal and spatial correlations between injection and seismicity are not created.

The IAR for the Redwater oilfield is close to zero, implying that evidence linking this operation to the seismicity is ambiguous. We note that some of the questions in the Verdon et al. (2019) framework pertain solely to the nature of the seismicity (for example, Q1), and for some questions (Q2, Q5) a positive answer will be obtained for any activity that happens to occur in the same place and at the same time as another seismogenic activity. This will serve to skew the IAR towards a positive value for any operation that happens to occur coincidentally near to

Table 2
Induced seismicity attribution results as applied to the Quest CCS and Redwater oil production activities.

Question	Score	Quest	Redwater
Q1. Has there been previous (either historical or instrumental) seismicity at the same site, or within the same regional setting?		Evidence Weighting (EW): 80 %	
Earthquakes have previously occurred in vicinity to the site, with similar rates and magnitudes	-5	No	No
Earthquakes have previously occurred within the same regional setting, with similar rates and magnitudes	-2	No	No
Earthquakes have not occurred at similar rates or magnitudes within the regional setting	+5	**Yes**	**Yes**
Past earthquakes occurred at similar depths within the regional setting	-3	No data	No data
Earthquakes are significantly shallower than any past events that have been observed within the regional setting	+3	No data	No data
Q2. Is there temporal coincidence between the onset of events and the industrial activities?		EW: 100 %	
The earthquake sequence began prior to the commencement of industrial activity	-15	No	No
The earthquake sequence did not begin until a significant period of time after the cessation of industrial activity	-5	No	No
The earthquake sequence began while the industrial activity was ongoing	+5	**Yes**	**Yes**
Q3. Are the observed seismic events temporally correlated with the injection or extraction activities?		EW: 80 %	
The earthquakes are coincident with the industrial activity, but there is minimal correlation	-4	No	**Yes**
There is some temporal correlation between the seismicity and the industrial activity	+4	**Yes**	No
There is strong temporal correlation between the seismicity and the industrial activity (e.g., between rates of injection and rates of seismicity)	+15	No	No
Q4. Do the events occur at similar depths to the activities?		EW: 80 %	
Earthquakes do not occur at the same depth, and there is no plausible mechanism by which stress or pressure changes could be transferred to these depths	-4	No	**Yes**
Earthquakes do not occur at the same depth, but plausible mechanisms exist by which stress or pressure changes could be transferred to these depths	+2	**Yes**	No
Earthquakes occur at similar depths to the industrial activity	+3	No	No
Q5. Is there spatial collocation between events and the activities?		100 %	
Earthquakes are distant to the activities, given the putative causative mechanism	-10	No	No
Earthquakes are sufficiently close to the activities, given the putative causative mechanism	+5	**Yes**	**Yes**
If earthquake loci change with time, this change is consistent with the industrial activity, for example, growing radially from a well or shifting in response to the start of a new well	+10	No	No
Q6. Is there a plausible mechanism to have caused the events?		EW: 80 %	
No significant pore-pressure increase or decrease occurred that can be linked in a plausible manner to the event hypocentral position	-5	No	**Yes**
Some pore-pressure or poroelastic stress change occurred that can be linked in a plausible manner to the event hypocentral position	+2	**Yes**	No
A large pore-pressure or poroelastic stress change occurred that can be linked in a plausible manner to the event hypocentral position	+5	No	No
Q7. Do the source mechanisms indicate an induced event mechanism?		EW 100 %	
The source mechanisms are consistent with the regional stress conditions	0	**Yes**	**Yes**
Source mechanisms are not consistent with the regional stress conditions, but are consistent with a putative causative mechanism (e.g., thrust faults above a subsiding reservoir)	+4	No	No

Table 3
Induced seismicity assessment outcomes.

	Quest	Redwater
ESR	84 %	84 %
IAR	+49 %	+8 %

another activity that is causing induced seismicity.

Oil production at Redwater has been ongoing for more than 65 years before the onset of any observed seismicity (of course, small events during the early life of the field could have been missed, but events with magnitudes $M_L \geq 2.5$ have been reported in the WCSB since the 1960s (Fereidoni and Cui, 2015), such that it is unlikely that moderate magnitude earthquakes at Redwater would have gone unnoticed). The nature of the operation is such that pressures have experienced a slight decrease relative to the initial reservoir conditions. Induced seismicity can occur in mature depleted hydrocarbon fields but is generally associated with very large pressure decreases and substantial compaction of the reservoir unit, which is not the case at Redwater. Very few cases of induced seismicity have been caused by water injection for secondary oil recovery and pressure maintenance (National Research Council, 2013). The Redwater reservoir, in the Leduc Formation, is hydraulically isolated from the basement by the Lotsberg Salts and Prairie Evaporites, and analysis of reflection seismic datasets in the area did not identify any faults penetrating these units (Shell Canada, 2015). As such, we conclude that waterflooding at the Redwater oilfield has not contributed to the observed seismicity. We note that induced seismicity has been generated by wastewater disposal into the Leduc Formation elsewhere in the WCSB (e.g., Schultz and Wang, 2020; Schultz et al., 2023), however these cases represent WWD rather than enhanced oil recovery, and also in these cases the Leduc Formation sits much closer to the Precambrian basement such that a direct hydraulic connection is more plausible.

5. Induced seismicity hazard

Having established that the observed seismicity is likely to have been caused by CO_2 injection at the Quest site, we now examine the implications with respect to induced seismicity hazard management. We begin by examining whether induced seismicity models would have been capable of forecasting the growing magnitudes of events in this sequence. We then make some recommendations with respect to ongoing management and mitigation of induced seismicity.

5.1. Induced seismicity forecasting

Fig. 4 shows the magnitude-frequency distribution for the observed earthquakes (using the AGS catalogue magnitudes). We find that the observed events are well-fitted by the Gutenberg and Richter (1944) relationship, with a *b* value of 0.53 (with the *b* value estimate being made using the Aki, 1965, maximum likelihood method). We see no evidence for an upper limit maximum magnitude truncation (Bommer and Verdon, 2024), implying that no geomechanical limit on the maximum possible magnitude has been reached (for contrary examples, see Schultz et al., 2025 and Verdon and Schultz, 2026).

Although no upper-limit maximum magnitude appears to have been reached, it is of interest to test the performance of magnitude forecasting models with respect to this sequence. We apply three different induced seismicity magnitude forecasting models which are widely used to characterise the hazard posed by ongoing induced seismicity sequences, including for other CCS operations in the WCSB (Verdon, 2016). Specifically, we seek to examine whether the seismicity has followed expected behaviours in terms of the growth of the largest observed magnitudes with time and could therefore have been forecastable. The models described below all aim to model the expected largest event that will occur during the sequence, which we refer to as M_{LRG} hereafter, noting that this is a different parameter to the largest possible event,

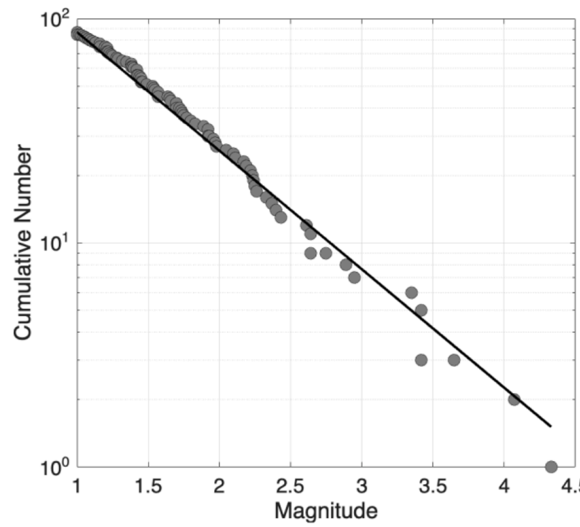

Fig. 4. Magnitude-frequency distribution for the observed seismicity (dots). The black line shows the fitted Gutenberg-Richter relationship.

M_{MAX} (see Bommer and Verdon, 2024).

Two of the models we use are based on establishing a link between injection rates and the seismicity and then extrapolating the relationship forward to future injection volumes. The seismogenic index, S_I, model of Shapiro et al. (2010) links the injected volume, ΔV, to the number of induced events N_E (above a given threshold magnitude, M):

$$S_I = \log_{10}\left(\frac{N_E}{\Delta V}\right) + bM, \quad (1)$$

where *b* is the Gutenberg-Richter *b*-value. The seismic efficiency model of Hallo et al. (2014) links the injected volume to the cumulative seismic moment, ΣM_0, released by the induced events:

$$S_E = \log_{10}\left(\frac{\Sigma M_0}{\mu \Delta V}\right), \quad (2)$$

where μ is the shear modulus, arbitrarily assumed here to be 20 GPa.

To apply these models, we follow the methodology described in Verdon et al. (2024). Our forecast proceeds on a prospective basis, where for each future time window (we use a 3-month time window here) our forecast largest expected event magnitude is based on the seismicity observed prior to this time window. For an upcoming time window, the additional expected seismicity is computed based on the planned injection volume and the current S_I or S_E value. Following Verdon et al. (2024), we use either cumulative or time-windowed S_I and S_E values. This additional seismicity is added to the past observed seismicity to produce an overall distribution, from which the largest expected magnitude is estimated based on the Gutenberg-Richter distribution (McGarr, 2014; van der Elst et al., 2016). To facilitate comparisons with S_I and S_E values observed at other sites, we convert the reported CO_2 injection rates, which are given in standard volumes, to the equivalent volume at reservoir temperatures and pressures using a density of 700 kg/m^3.

The third model we use is based on extreme value (EV) statistics, as described in Verdon and Eisner (2024). This method is based on the theory of extreme value estimators (Cooke, 1979). These methods rely solely on the statistical properties of the observed sequence, and do not involve any reference to injection rates or any other subsurface information. Verdon and Eisner (2024) adapted these methods to produce an empirically constrained approach using a large number of observed induced seismicity sequences. For this model, for each upcoming time window the expected largest magnitude event is estimated from the population of events occurring prior to the start of this window.

The AGS catalogue only provides events above $M_L \geq 1.0$. In the magnitude-frequency plot (Fig. 4) we do not see any lower magnitude truncation from a minimum magnitude of completeness, M_C, within the available data range, implying that $M_C \leq 1.0$. However, examination of the time evolution of the seismicity (Fig. 5) shows that no events with $M_L < 1.5$ were recorded prior to 2024. This implies that the detection capabilities may have improved through time, such that a value of $M_C \leq 1.0$ is not appropriate prior to 2024. There are insufficient events to produce a robust statistical estimate for M_C prior to 2024. Hence, in this analysis we adopt a value of $M_C = 1.5$, noting that the S_I, S_E, and EV methods are primarily sensitive to the largest events within a sequence, and so are relatively insensitive to the choice of M_C value.

Fig. 5a shows the time-windowed and cumulative S_I and S_E values, while Fig. 5b shows the resulting forecasts using these methods. Fig. 5c shows the forecast results using the EV method. We see that the S_E model significantly underpredicts the $M_L \geq 4.0$ events in April/May 2026.

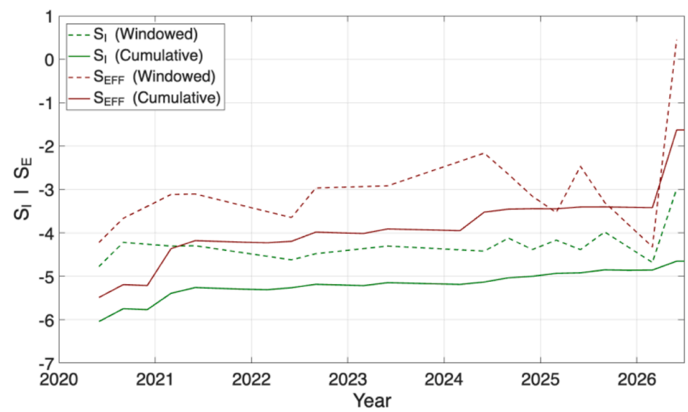

(a)

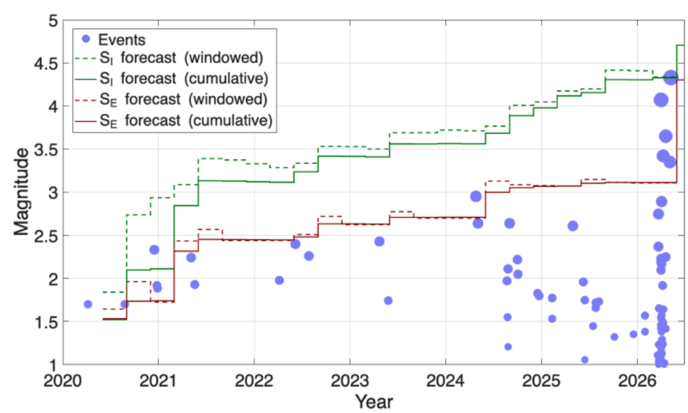

(b)

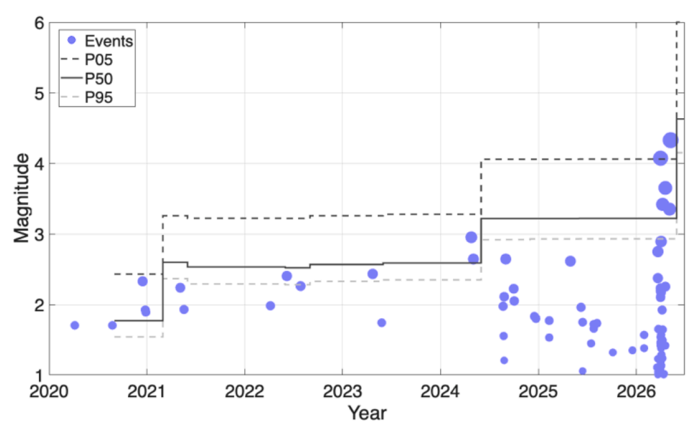

(c)

Fig. 5. Induced seismicity magnitude forecasting models applied to the Quest events. In (a) we show the evolution of the time-windowed and cumulative S_I and S_E parameters. In (b) we show the resulting largest expected event magnitude forecasts using these models. In (c) we show the largest expected event magnitude forecasts using the EV method: the solid line shows the magnitude with a 50 % chance of exceedance, while the dark and light dashed lines show the 5 % and 95 % thresholds, respectively.

However, $M_L \geq 4.0$ events are close to the most likely largest event magnitude estimated by the S_I model, and close to the upper confidence interval (5 % chance of exceedance) for the EV model.

The S_I model and the Verdon and Eisner (2024) EV model both allow the user to characterise a probability distribution for M_{LRG}. To further investigate the performance of these two models, in Fig. 6 we show the probability distributions produced by these models for M_{LRG} at the timestep prior to the occurrence of the $M_L \geq 4.0$ events in April/May 2026. We can therefore compare the probability distributions computed for the largest expected magnitudes immediately prior to the M_L 4.0 events that subsequently occurred.

We see that the EV method has an exceedance probability of c. 5 % for an M_L 4.0 event – the observed event is therefore at the upper end of the EV forecast, but within reasonable bounds in terms of probability. The S_I model has an exceedance probability of c. 80 % for an M_L 4.0 event – the observed event is therefore towards the centre of the S_I model forecast. However, we note that the range of the S_I forecast in this case is relatively large: the 5 % to 95 % confidence interval spans a range of over three magnitude units. It is debatable whether in practice an operational forecast spanning this range (i.e., being told "your next largest induced event could be between M_L 3 to M_L 7.0") would provide actionable information to an operator seeking to manage induced seismicity risks. It is therefore encouraging that, in this case, the EV method provided a more tightly constrained forecast, with the 5 % to 95 % confidence interval for M_{LRG} spanning from $2.9 \leq M_{LRG} \leq 4.0$. This forecast nevertheless covered the seismicity that was ultimately observed and could therefore have provided actionable information to the operator.

Of course, the choice of whether to act on any induced seismicity forecasting model will depend not only on the output of the model (i.e., the likelihood of exceedance of a given magnitude), but on the expected impacts from an event of a given magnitude (e.g., the potential for nuisance and/or damage, as described in Schultz et al., 2020), and the appetite for risk of the operator and the regulator (which is assumed to represent the public interest), especially when viewed with respect to the economic or social benefits of the operation in question. We note that CCS operations are intended to mitigate the severe impacts of anticipated future climate change which, from a global perspective, are expected to far outweigh the local nuisance posed by moderate magnitude induced seismic events (we are not aware of any damage reported from the events reported in this study).

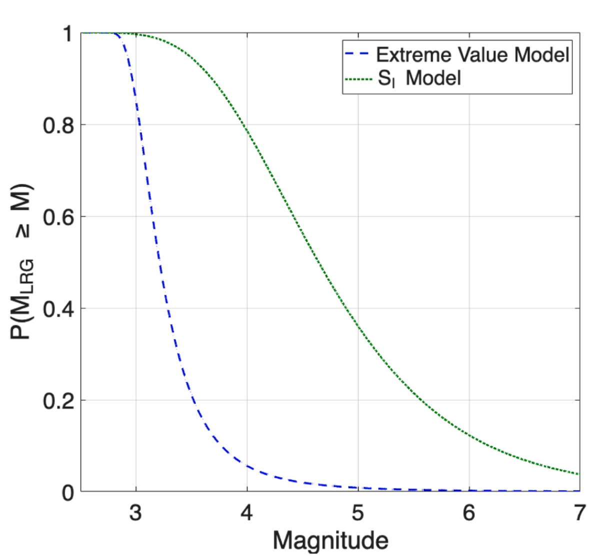

Fig. 6. Probability distributions for the largest expected magnitude produced by the S_I model (green) and extreme value model (blue) at the timestep prior to the occurrence of the $M_L \geq 4.0$ events in April/May 2026.

5.2. Induced seismicity mitigation

Injection-induced seismicity is typically generated by pressure increases de-clamping critically stressed faults. The prevalence of induced seismicity is therefore determined by (i) the abundance of pre-existing faulting, (ii) the in-situ stress conditions, and (iii) the amplitude and spatial dimensions of pressure perturbations generated by injection (Verdon and Rodríguez-Pradilla, 2023). The first two of these factors are controlled by the geological conditions and cannot be affected by operational controls. Mitigation of induced seismicity therefore depends on successful pressure management, or at least ensuring that elevated pressures are not able to reach critically stressed faults. Evidently this can be achieved by stopping injection operations, but this is an unattractive option given the level of investment in large scale CCS projects, and the societal importance of reducing global CO_2 emissions.

Elsewhere, induced seismicity at large-scale fluid injection sites has been controlled by, for example, reducing the rate of injection (e.g., OCC, 2016), or conducting regular pauses in injection to allow pressures to dissipate (Ake et al., 2005). It is commonly assumed that rates of induced seismicity scale with the rate of pressure increase (e.g., Langenbruch et al., 2018; Hill et al., 2024; Verdon et al., 2024). Field-scale reservoir simulations can be used to model how reductions in injection rate will influence the future rate of subsurface pressure change, such that a suitable rate can be identified that maximises the total injected volume while ensuring that seismicity remains within acceptable levels (Hill et al., 2024).

In extremis, subsurface pressure could be managed by extracting water from the target CCS formation. This would create a secondary challenge because a disposal pathway for the produced water would need to be identified. Produced water could be re-injected into shallower formations that are hydraulically disconnected from the basement: a significant portion of wastewater disposal from oilfield operations in the WCSB takes place into shallower, Cretaceous-age strata without causing any reported cases of induced seismicity (Verdon et al., 2016). Deeper formations are generally preferred for CCS operations because (i) CO_2 becomes denser with increasing pressure, enabling greater storage per unit volume, and (ii) deep formations have more barriers to upward migration of buoyant CO_2 back to the surface. These factors are less relevant for re-injection of produced water, which is much less compressible, and which is not buoyant (and so the need for sealing caprock layers is reduced).

Moving the injection to shallower depths, away from crystalline basement rocks, has been successful in mitigating induced seismicity in some cases (e.g., Yeck et al., 2016): this approach was used to mitigate induced seismicity at the Decatur CCS project (Hosseini et al., 2022). In the WCSB, and for many cases elsewhere, the prevalence of induced seismicity is strongly linked to the proximity to crystalline basement rocks (e.g., Hincks et al., 2018; Pawley et al., 2018; Wozniakowska and Eaton, 2020; Verdon and Rodríguez-Pradilla, 2023). In general, we expect crystalline basement rocks to be stiffer, to be more stressed, and to contain more and larger faults, and therefore to be more prone to induced seismicity. Faults in shallower sedimentary formations may be strata-bound, which will limit the maximum size of induced earthquakes that can be generated (e.g., Verdon and Schultz, 2026). Identification of potential target layers for CO_2 injection (or for re-injection of water that has been produced for pressure management of deeper CO_2 injection) that are hydraulically isolated from the basement may therefore be an important strategy to mitigate induced seismicity during future CCS operations.

We note that the statistical models we used to forecast induced seismicity magnitudes (Section 5.1) are based on the assumption that the seismicity is produced by a constant underlying geomechanical process, such that preceding seismicity can be used to characterise upcoming events. If CO_2 injection is re-started under different conditions (for example, with reduced rates or pressures, with proactive pressure management, or at shallower depths) then the previous seismicity may not suitably characterise upcoming events, in which case the forecasting models will need to be recalibrated with ongoing microseismic observations. In many cases of induced seismicity, we have seen the levels of seismicity stabilise and reduce over time (Rodríguez-Pradilla et al., 2022), especially in response to various mitigating measures (Verdon et al., 2024). However, it is also possible that, if the pressure pulse created by CO_2 injection continues to grow outwards, it may perturb additional critically stressed faults, leading to further felt events.

6. Conclusions

We have applied an induced seismicity attribution scheme to the sequence of earthquakes to the NE of Edmonton, Alberta that has been reported in the AGS catalogue since 2020 (with the first microseismic events being identified in 2016). In doing so, we have computed earthquake focal depths and source mechanisms for the largest events in the sequence. As potential causes, we considered CO_2 injection at the Quest CCS site and oil production under waterflooding at the Redwater oilfield. We conclude that the earthquakes are likely to have been induced by the CCS operations at Quest. We also concluded that nearby oilfield operations are Redwater did not contribute to the seismicity. The $M_L \geq 4.0$ earthquakes in April and May 2026 therefore represent the first reported case where CCS operations have caused induced seismicity of sufficient magnitude to be widely felt.

We applied several induced event magnitude forecasting models to the seismic sequence. We found that the S_E model significantly underpredicted the $M_L \geq 4.0$ events. These events were, however, within the forecast ranges produced by the S_I and EV models. That said, the S_I model produced an extremely broad forecast window that may be of limited utility for operational decision making. The strong performance of the EV model is consistent with past comparisons of performance between volume-based (i.e., S_I or S_E) versus EV-based models (Verdon and Eisner, 2024).

We conclude by considering options for ongoing induced seismicity management. Reductions in injection rates, which in turn reduce the rates of pressure increase, have proven successful in mitigating induced seismicity in other cases. Our hypocentral depth estimates indicate that the events are located within the underlying crystalline basement. Injection (either of CO_2, or of water that is produced in order to manage pressures in the BCS) into strata that are hydraulically isolated from the basement represents another potential strategy for induced seismicity management. If mitigation measures are applied to future CO_2 injection, then models for induced seismicity hazard should be updated based on ongoing seismicity observations that characterise the response of the seismicity to the mitigation actions.

Data and resources

The earthquake catalog used in this study was accessed via the Alberta Earthquake Dashboard (AGS, 2020). The waveforms used in the source mechanism inversion were obtained via IRIS (https://www.iris.edu/hq/). The network and station codes are provided in Fig. 3.

CRediT authorship contribution statement

James P. Verdon: Writing – original draft, Supervision, Project administration, Methodology, Funding acquisition, Formal analysis, Conceptualization. **Cindy S.Y. Lim:** Writing – review & editing, Formal analysis, Data curation. **Germán Rodríguez-Pradilla:** Writing – review & editing, Data curation.

Declaration of competing interest

The authors declare the following financial interests/personal relationships which may be considered as potential competing interests:

The authors report that financial support was provided by the Bristol and Oxford Passive Seismic (BOPS) Research Consortium, which is funded by a collection of energy operating companies and service providers, many of whom have CCS activities as part of their business. James Verdon has acted as an independent consultant for organisations including energy operating companies and governmental organisations on issues pertaining to induced seismicity.

Acknowledgements

The authors received funding to support this study from the UK Natural Environment Research Council (NERC) SeisGreen Grant (Grant Number NE/W009293/1) and the Engineering and Physical Sciences Research Council (EPSRC) DarkSeis Grant (Grant Number EP/Y020960/1). This work was also supported by the Bristol and Oxford Passive Seismic (BOPS) research project, which is supported by industry operating companies and service providers.

Supplementary materials

Supplementary material associated with this article can be found, in the online version, at doi:10.1016/j.ijggc.2026.104796.

Data availability

The earthquake catalog was accessed via the Alberta Earthquake Dashboard (AGS, 2020). The waveforms used in the source mechanism inversion were obtained via IRIS (https://www.iris.edu/hq/).

References

AER, 2026. Directive 065: Resources Applications for Oil and Gas Reservoirs. Alberta. Energy Regulator Directive 065, 294. Accessed at: https://static.aer.ca/prd/documents/directives/Directive065.pdf. on 10/06/2026.

AGS, 2020. Alberta earthquake dashboard, IAM 005. Accessed at: https://ags.aer.ca/publications/all-publications/iam-005. on 10/06/2026.

Ake, J., Mahrer, K., O'Connell, D., Block, L., 2005. Deep-injection and closely monitored induced seismicity at Paradox Valley, Colorado. Bull. Seismol. Soc. Am. 95, 664–683.

Aki, K., 1965. Maximum likelihood estimate of b in the formula log N = a – bM and its confidence limits. Bulletin of the Earthquake, 43. Research Institute, University of Tokyo, pp. 237–239.

BEIS, 2019. Government ends support for fracking: press release from the UK Department of Business. Energy and Industrial Strategy. Accessed at: https://www.gov.uk/government/news/government-ends-support-for-fracking on 10/06/2026.

Bommer, J.J., Verdon, J.P., 2024. The maximum magnitude of natural and induced earthquakes. Geomech. Geophys. Geo-energy Geo-resour. 10, 172.

Campbell, N.M., Leon-Corwin, M., Ritchie, L.A., Vickery, J., 2020. Human-induced seismicity: risk perceptions in the state of Oklahoma. Extr. Ind. Soc. 7, 119–126.

Cooke, P., 1979. Statistical inference for bounds of random variables. Biometrica 66, 367–374.

Cremen, G., Werner, M.J., 2020. A novel approach to assessing nuisance risk from seismicity induced by UK shale gas development, with implications for future policy design. Nat. Hazards Earth Syst. Sci. 20, 2701–2719.

CTV, 2026. 4.5-magnitude earthquake shakes central Alberta residents, cause under investigation. CTV News. Accessed at: https://www.ctvnews.ca/edmonton/article/45-magnitude-earthquake-shakes-central-alberta-residents-as-cause-under-investigation/. on 10/06/2026.

Dando, B.D.E., Goertz-Allmann, B.P., Kühn, D., Langet, N., Dichiarante, A.M., Oye, V., 2021. Relocating microseismicity from downhole monitoring of the Decatur CCS site using a modified double-difference algorithm. Geophys. J. Int. 227, 1094–1122.

Davis, S.D., Pennington, W.D., 1989. Induced seismic deformation in the Cogdell oil field of west Texas. Bull. Seismol. Soc. Am. 79, 1477–1494.

Fereidoni, A., Cui, L., 2015. Composite Alberta seismicity catalog: CASC2014-x. Accessed at: https://www.inducedseismicity.ca/wp-content/uploads/2015/01/Composite-Alberta-Seismicity-Catalog3.pdf on 22/06/2026.

Gan, W., Frohlich, C., 2013. Gas injection may have triggered earthquakes in the Cogdell oil field, Texas. Proc. Natl. Acad. Sci. 110, 18786–18791.

Glubokovskikh, S., Saygin, E., Shapiro, S., Gurevich, B., Isaenkov, R., Lumley, D., Nakata, R., Drew, J., Pevzner, R., 2022. A small CO_2 leakage may induced seismicity on a sub-seismic fault in a good-porosity clastic saline aquifer. Geophys. Res. Lett. 49, e2022GL098062.

Goertz-Allmann, B.P., Langet, N., Iranpour, K., Kühn, D., Baird, A., Oates, S., Rowe, C., Harvey, S., Oye, V., Nakstad, H., 2024. Effective microseismic monitoring of the Quest CCS site, Alberta, Canada. Int. J. Greenh. Gas Control 133, 104100.

Grasso, J.-R., Amorese, D., Karimov, A., 2021. Did wastewater disposal drive the longest seismic swarm triggered by fluid manipulations? Lacq, France, 1969-2016. Bull. Seismol. Soc. Am. 111, 2733–2752.
Gutenberg, B., Richter, C.F., 1944. Frequency of earthquakes in California. Bull. Seismol. Soc. Am. 34, 185–188.
Hallo, M., Oprsal, I., Eisner, L., Ali, M.Y., 2014. Prediction of magnitude of the largest potentially induced seismic event. J. Seismol. 18, 421–431.
Heimann, S., Isken, M., Kühn, D., Sudhaus, H., Steinberg, A., Daout, S., Cesca, S., Bathke, H., Dahm, T., 2018. Grond: A probabilistic earthquake source inversion framework. GFZ Data Services. https://doi.org/10.5880/GFZ.2.1.2018.003.
Hill, R.G., Weingarten, M., Langenbruch, C., Fialko, Y., 2024. Mitigation and optimization of induced seismicity using physics-based forecasting. J. Geophys. Res. 129, e2024JB028759.
Hincks, T., Aspinall, W., Cooke, R., Gernon, T., 2018. Oklahoma's induced seismicity strongly linked to wastewater injection depth. Science 359, 1251–1255.
Hosseini, S., Horvorka, S., Savvaidis, A., Kavoura, F., Nicot, J.-P., 2022. Current State of Knowledge Regarding the Risk of Induced Seismicity at CO_2 Storage Projects. International Energy Agency Greenhouse Gas R&D Programme. Accessed at: https://ieaghg.org/publications/current-state-of-knowledge-regarding-the-risk-of-induced-seismicity-at-co2-storage-projects/ on 18/06/2026.
Igonin, N., Verdon, J.P., Kendall, J.-M., Eaton, D.W., 2021. Large-scale fracture systems are permeable pathways for fault activation during hydraulic fracturing. J. Geophys. Res. 126, e2020JB020311.
Igonin, N., Verdon, J.P., Eaton, D.W., 2022. Seismic anisotropy reveals stress changes around a fault as it is activated by hydraulic fracturing. Seismol. Res. Lett. 93, 1737–1752.
Jacquemond, L., Letort, J., Cotton, F., Causse, M., Grasso, J.R., Senechal, G., Ammirati, J. B., Derode, B., Grimaud, F., Pauchet, H., Benhamed, S., Sylvander, M., 2024. Analysing 50 yr of the Lacq induced seismicity (southwestern France) highlights the role of fluid injection. Geophys. J. Int. 238, 214–234.
Langenbruch, C., Shapiro, S., 2025. In: Seismogenic index model of seismicity induced by CO_2 storage operations: 86th EAGE Annual Conference Toulouse, Expanded Abstracts. https://doi.org/10.3997/2214-4609.2025101621.
Langenbruch, C., Weingarten, M., Zoback, M.D., 2018. Physics-based forecasting of man-made earthquake hazards in Oklahoma and Kansas. Nat. Commun. 9, 3946.
Lee, K.K., Ellsworth, W.L., Giardini, D., Townend, J., Ge, S., Shimamoto, T., Yeo, I.-W., Kang, T.-S., Rhie, J., Sheen, D.-H., Chang, C., Woo, J.-U., Langenbruch, C., 2019. Managing injection-induced seismic risks. Science 364, 730–732.
McCafferty, A.E., San, C.A., Lawley, C., Graham, G.E., Gadd, M.G., Huston, D.L., Kelley, K.D., Paradis, S., Peter, J.M., Czarnota, K., 2025. Shapefiles of faults for the United States, Canada, and Australia. U.S. Geological Survey data release. https://doi.org/10.5066/P970GDD5.
McGarr, A., 2014. Maximum magnitude earthquakes induced by fluid injection. J. Geophys. Res. 119, 1008–1019.
National Research Council, 2013. Induced Seismicity Potential in Energy Technologies. The National Academies Press, Washington DC.
OCC, 2016. Media advisory - Regional earthquake response plan for western Oklahoma. Oklahoma Corporation Commission, Oklahoma City, OK. Accessed at: https://oklahoma.gov/content/dam/ok/en/occ/documents/ajls/news/2016/02-16-16westernregionalplan.pdf. on 19/06/2026.
Oprsal, I., Eisner, L., 2014. Cross-correlation – an objective tool to indicate induced seismicity. Geophys. J. Int. 196, 1536–1543.
Paap, B., Verdel, A., Meekes, S., Steeghs, P., Vandeweijer, V., Neele, F., 2014. Four years of experience with a permanent seismic monitoring array at the Ketzin CO_2 storage pilot site. Energy Procedia 63, 4043–4050.
Pawley, S., Schultz, R., Playter, T., Corlett, H., Shipman, T., Lyster, S., Hauck, T., 2018. The geological susceptibility of induced earthquakes in the Duvernay Play. Geophys. Res. Lett. 45, 1786–1793.
Payre, X., Maisons, C., Marblé, A., Thibeau, S., 2014. Analysis of the passive seismic monitoring performance at the Rousse CO_2 storage demonstration pilot. Energy Procedia 63, 4339–4357.
Reiter, K., Heidbach, O., Schmitt, D., Haug, K., Ziegler, M., Moeck, I., 2014. A revised crustal stress orientation database for Canada. Tectonophysics 636, 111–124.
Rodríguez-Pradilla, G., Eaton, D.W., Verdon, J.P., 2022. Basin-scale multi-decadal analysis of hydraulic fracturing and seismicity in western Canada shows non-recurrence of induced runaway fault rupture. Scientific Reports 12, 14463.
Rutledge, J., Soma, N., 2010. Microseismic monitoring of CO_2 enhanced oil recovery in the Aneth Field. In: Rutledge, J. (Ed.), Geologic demonstration at the Aneth Oil Field, Paradox Basin, Utah. New Mexico Institute of Mining and Technology, Socorro, New Mexico.
Schultz, R., Stern, V., 2015. The regional Alberta Observatory for earthquake studies network (RAVEN). Can. Soc. Explor. Geophys. Rec. 40, 34–37.
Schultz, R., Telesca, L., 2018. The cross-correlation and reshuffling tests in discerning induced seismicity. Pure Appl. Geophys. 175, 3395–3401.
Schultz, R., Wang, R., 2020. Newly emerging cases of hydraulic fracturing induced seismicity in the Duvernay East Shale Basin. Tectonophysics 779, 228393.
Schultz, R., Beroza, G., Ellsworth, W., Baker, J., 2020. Risk-informed recommendations for managing hydraulic fracturing-induced seismicity via traffic light protocols. Bull. Seismol. Soc. Am. 110, 2411–2422.
Schultz, R., Woo, J.-U., Pepin, K., Ellsworth, W.L., Zebkar, H., Segall, P., Gu, Y.J., Samsonov, S., 2023. Disposal from in situ bitumen recovery induced the M_L 5.6 Peace River earthquake. Geophys. Res. Lett. 50, e2023GL102940.
Schultz, R., Lanza, F., Dyer, B., Karvounis, D., Fiori, R., Shi, P., Ritz, V., Villiger, L., Meier, P., Weimer, S., 2025. The bound growth of induced earthquakes could de-risk hydraulic fracturing. Commun. Earth Environ. 6, 995.
Schultz, R.J., Yusifbayov, J., Shipman, T.C., 2020. The scientific induced seismicity monitoring network (SCISMN). AER/AGS Open File Report 2019-09. Accessed at: https://ags.aer.ca/publications/all-publications/ofr-2019-09. on 19/08/2026.
Shapiro, S.A., Dinske, C., Langenbruch, C., Wenzel, F., 2010. Seismogenic index and magnitude probability of earthquakes induced during reservoir fluid stimulations. Lead. Edge 29, 304–308.
Shell Canada, 2013. Quest Carbon Capture and Storage Project Measurement, Monitoring and Verification plan. Accessed at: https://open.alberta.ca/publications/quest-carbon-capture-and-storage-project-report-2012 on 22/06/2026.
Shell Canada, 2015. Quest Carbon Capture and Storage Project Annual Summary Report, 2024. Alberta Department of Energy. Accessed at: https://open.alberta.ca/publications/quest-carbon-capture-and-storage-project-report-2014. on 10/06/2026.
Shell Canada, 2025a. Quest Carbon Capture and Storage Project Annual Summary Report, 2024. Alberta Department of Energy. Accessed at: https://open.alberta.ca/publications/quest-carbon-capture-and-storage-project-annual-report-2024 on 10/06/2026.
Shell Canada, 2025b. Quest carbon capture and storage project 2024 annual status report Accessed at: https://open.alberta.ca/publications/quest-carbon-capture-and-storage-project-annual-report-2024 on 10/06/2026.
Stork, A.L., Verdon, J.P., Kendall, J.-M., 2015. The microseismic response at the in Salah carbon capture and storage (CCS) site. Int. J. Greenh. Gas Control 32, 159–171.
van der Elst, N.J., Page, M.T., Weiser, D.A., Goebel, T.H.W., Hosseini, S.M., 2016. Induced earthquake magnitudes are as large as (statistically) expected. J. Geophys. Res. 121, 4575–4590.
van de Graaff, W.J.E., van Geuns, L., Boersma, T., 2018. The termination of Groningen gas production – background and next steps. Columbia Sch. Int. Public Aff. Cent. Glob. Energy Policy.
Verdon, J.P., 2014. Significance for secure CO_2 storage of earthquakes induced by fluid injection. Environ. Res. Lett. 9, 064022.
Verdon, J.P., 2016. Using microseismic data recorded at the Weyburn CCS-EOR site to assess the likelihood of induced seismic activity. Int. J. Greenh. Gas Control 54, 421–428.
Verdon, J.P., Bommer, J.J., 2021. Green, yellow, red, or out of the blue? An assessment of traffic light schemes to mitigate the impact of hydraulic fracturing-induced seismicity. J. Seismol. 25, 301–326.
Verdon, J.P., Rodríguez-Pradilla, G., 2023. Assessing the variability in hydraulic fracturing-induced seismicity occurrence between North American shale plays. Tectonophysics 859, 229898.
Verdon, J.P., Eisner, L., 2024. An empirically constrained forecasting strategy for induced earthquake magnitudes using extreme value theory. Seismol. Res. Lett. 95, 3278–3294.
Verdon, J.P., Schultz, R., 2026. Induced earthquakes in the southern Delaware Basin, Texas, are bound by a geomechanically controlled maximum magnitude. Geophys. Res. Lett. 53, e2025GL117419.
Verdon, J.P., Kendall, J.-M., White, D.J., Angus, D.A., 2011. Linking microseismic event observations with geomechanical models to minimise the risks of storing CO_2 in geological formations. Earth Planet. Sci. Lett. 305, 143–152.
Verdon, J.P., Kendall, J.-M., Stork, A.L., Chadwick, R.A., White, D.J., Bissell, R.C., 2013. A comparison of geomechanical deformation induced by 'megatonne' scale CO_2 storage at Sleipner, Weyburn and in Salah. Proc. Natl. Acad. Sci. 110, E2762–E2771.
Verdon, J.P., Stork, A.L., Bissell, R.C., Bond, C.E., Werner, M.J., 2015. Simulation of seismic events induced by CO_2 injection at in Salah. Algeria: Earth Planet. Sci. Lett. 426, 118–129.
Verdon, J.P., Kendall, J.-M., Horleston, A.C., Stork, A.L., 2016. Subsurface fluid injection and induced seismicity in southeast Saskatchewan. Int. J. Greenh. Gas Control 54, 429–440.
Verdon, J.P., Baptie, B.J., Bommer, J.J., 2019. An improved framework for discriminating seismicity induced by industrial activities from natural earthquakes. Seismol. Res. Lett. 90, 1592–1611.
Verdon, J.P., Pullen, B., Rodriguez-Pradilla, G., 2024. Growth and stabilisation of induced seismicity rates during long-term, low pressure fluid injection. Philos. Trans. R. Soc. A 382, 20230183.
Verdon, J.P., Boeckx, D., Fox, A., Marshall, F., Pooladi-Darvish, M., Watson, N., 2026. Detailed seismological observations from the M 5.6 Reno earthquake sequence, the largest induced seismic event in Canada. Seismol. Res. Lett. in press.
Wozniakowska, P., Eaton, D.W., 2020. Machine learning-based analysis of geological susceptibility to induced seismicity in the Montney formation. Canada: Geophys. Res. Lett. 47, e2020GL089651.
Yeck, W.L., Sheehan, A.F., Benz, H.M., Weingarten, M., Nakai, J., 2016. Rapid response, monitoring, and mitigation of induced seismicity near Greeley, Colorado. Seismol. Res. Lett. 87, 837–847.
Yu, H., Kao, H., Wang, B., Visser, R., 2022. Long-term fluid injection can expedite fault reactivation and development: riedel shear structures illuminated by induced earthquakes in Alberta. Canada: J. Geophys. Res. 127, e2022JB025126.
Zoback, M.D., Gorelick, S.M., 2012. Earthquake triggering and large-scale geologic storage of carbon dioxide. Proc. Natl. Acad. Sci. 109, 10164–10168.
Zoback, M., Hennings, P., 2025. Implications of earthquakes triggered by massive injection of produced water in saline aquifers for large-scale geologic storage of CO_2. Int. J. Greenh. Gas Control 146, 104447.